Gondwana Research 116 (2023) 1–11

Contents lists available at ScienceDirect

Gondwana Research

journal homepage: www.elsevier.com/locate/gr

Astrochronology and carbon-isotope stratigraphy of the Fengcheng Formation, Junggar Basin: Terrestrial evidence for the Carboniferous-Permian Boundary

Renda Huang [a,b], Fujie Jiang [a,b,*], Di Chen [a,b], Ruoyuan Qiu [c,d], Tao Hu [a,b], Linhao Fang [a,b], Meiling Hu [a,b], Guanyun Wu [a,b], Chenxi Zhang [a,b], Jiahao Lv [a,b], Yuping Wu [a,b], Liliang Huang [e]

[a] State Key Laboratory of Petroleum Resources and Prospecting, China University of Petroleum (Beijing), Beijing 102249, China
[b] College of Geosciences, China University of Petroleum (Beijing), Beijing 102249, China
[c] Key Laboratory of Cenozoic Geology and Environment, Institute of Geology and Geophysics, Chinese Academy of Sciences, Beijing, China
[d] University of Chinese Academy of Sciences, Beijing, China
[e] Research Institute of Petroleum Exploration and Development, Xinjiang Oilfield Company, CNPC, Karamay 834000, Xinjiang, China

ARTICLE INFO

Article history:
Received 28 June 2022
Revised 4 December 2022
Accepted 31 December 2022
Available online 3 January 2023
Handling Editor: Sanghoon Kwon

Keywords:
Carboniferous-Permian Boundary
Astrochronology
Negative carbon isotope excursion
Fengcheng Formation
Junggar Basin

ABSTRACT

The Carboniferous–Permian Boundary (CPB) is a major stratigraphic boundary and a marker for global stratigraphic correlation. However, the delimitation and global correlation of the CPB is hindered by the erosion during the Late Paleozoic Ice Age. Several carbonate platforms show a negative carbon isotope excursion (NCIE) in response to the CPB, which has great potential for the delimitation of this boundary. However, the response of terrestrial profiles to the CPB is unclear, and the global synchroneity of this NCIE is controversial. We studied a high paleolatitude section to evaluating the feasibility of the NCIE for delimitating CPB. We used astrochronological analysis of the 340 m Gamma Ray log of the Fengcheng Formation in Mahu Sag, Junggar Basin, northwest China, where the CPB may have been recorded. We constructed a high-resolution chronostratigraphic framework for the Fengcheng Formation, which precisely defines the chronostratigraphic attribution of the Fengcheng Formation as the Gzhelian–Asselian, and confirms that the CPB is recorded in the Fengcheng Formation. In addition, a global correlation of carbon isotope profiles revealed a negative excursion in terrestrial carbon isotope profiles across the CPB, which is consistent with the characteristics of NCIEs in several marine profiles. The similarity of the NCIE records supports their global synchrony and confirms that they can be used to delimit the CPB in terrestrial sections. Combining the astronomical time scale and the carbon isotope profile, we constrain the position of the CPB to the depth range of 4694.84–4703.56 m, with 4698.9 m as a preliminary estimate of the CPB. This new astronomical timescale and the stratigraphic position of the CPB enable the revision of the chronostratigraphic attribution of the terrestrial strata in the Junggar Basin. Overall, our results contribute to studies of the Carboniferous–Permian global carbon cycle, high-latitude glaciation, eustatic fluctuations, global volcanism, and their potential relationships.

1. Introduction

The Late Paleozoic Ice Age (LPIA, ~360–260 Ma) was the longest Phanerozoic icehouse period and it provides a deep-time perspective for understanding the coupling of climate and glaciation as well as possible future anthropogenic climate change (Fielding et al., 2008; Isbell et al., 2003). The LPIA led to the growth and shrinkage of the Gondwana ice sheets; however, the climatic response to the LPIA at high latitudes of the Northern Hemisphere is unclear, and a transition model between glacial and interglacial periods has not yet been established, and therefore the coevolution of climate and glaciation during the LPIA requires further investigation (Buggisch et al., 2011; Fielding et al., 2008; Isbell et al., 2003; Montañez and Poulsen, 2013; Wang et al., 2021). Understanding the global climatic response to the LPIA is hindered by the difficulty of stratigraphic correlation between different regions. The Carboniferous–Permian Boundary (CPB, 298.9 ± 0.15 Ma; cited from the GTS2020 time scale) is defined by the first occurrence of the conodont *Streptognathodus isolatus* in the *S. wabaunsensis* chronocline (Aretz et al., 2020; Davydov et al., 1998; Cohen et al.,

* Corresponding author at: State Key Laboratory of Petroleum Resources and Prospecting, China University of Petroleum (Beijing), Beijing 102249, China.
E-mail address: jiangfj@cup.edu.cn (F. Jiang).

https://doi.org/10.1016/j.gr.2022.12.016
1342-937X/

2021), which is a typical stratigraphic boundary and evidence for global stratigraphic correlation. The growth of large ice sheets and glacial and interglacial cyclicity during the Late Paleozoic Ice Age (LPIA, ~360–260 Ma) led to frequent global eustatic and climatic fluctuations, causing the exposure and erosion of Carboniferous sediments in several regions (Buggisch et al., 2011; Fielding et al., 2008; Isbell et al., 2003; Montañez and Poulsen, 2013; Wang et al., 2021). Previous studies of terrestrial sections have tended to use unconformities (e.g., in the Junggar Basin: Buckman et al., 2004; He et al., 2018) and coal seams (e.g., in the Ordos Basin: Kuang et al., 2020) to define the CPB. Thus, few detailed studies have been conducted of the CPB, which hinders its precise delimitation and global correlation. Previous research has identified a negative carbon isotope excursion (NCIE) close to the CPB in several continuous Carboniferous–Permian profiles (e.g., Peters-Kottig et al., 2006), and this NCIE is potentially important for delimiting the CPB. However, most previous studies have focused on marine rather than on terrestrial records, and the global synchroneity of the NCIE needs to be confirmed.

Stratigraphic age calibration methods based on astronomical cycles have been widely used to establishment chronostratigraphic frameworks (Hinnov, 2012; Strasser et al., 2006; Shi et al., 2019). Astronomically-forced climatic cycles can be recovered using paleoclimate proxies and used to build a continuous high-resolution time scale (Gong and Li, 2020; Shi et al., 2021; Ma et al., 2019). Biostratigraphic and radioisotope chronology studies have confirmed that astronomical cycles are present in Paleozoic sediments (e.g., De Vleeschouwer et al., 2017; Wu et al., 2018; Hinnov and Diecchio, 2020). Because of its advantages for chronostratigraphic age calibration, astronomical analysis provides a potentially powerful tool for the high-resolution delimitation of the CPB.

The drill cores in the Late Paleozoic Fengcheng Formation in Mahu Sag in the Junggar Basin provide a high-paleolatitude deep-time perspective for studying the terrestrial stratigraphic response to the CPB (Fig. 1). Previous studies in the Junggar Basin tended to regard the unconformity between the marine basement and the terrestrial strata as the CPB (e.g., Buckman et al., 2004; He et al., 2018). However, several recent studies have suggested that the CPB is preserved near the base of the Fengcheng Fm, and therefore that a continuous Carboniferous–Permian profile exists in Mahu Sag (Gao et al., 2020; Huang et al., 2021; Wang et al., 2022). However, the precise stratigraphic position of the CPB in Mahu Sag has not been determined, and an unequivocal signature of the CPB in terrestrial strata had yet to be determined. Here, we present the results of a detailed astrochronological analysis and a carbon isotope profile of the Fengcheng Fm in Mahu Sag, with the objectives of producing a terrestrial record of the CPB and potentially to provide new evidence for its delimitation. Our results facilitate the correlation and comparison of Carboniferous–Permian stratigraphy and contribute to a better understanding of the global climate response of the LPIA from the Late Carboniferous to the Early Permian.

2. Geological setting

The Junggar Basin is a major superimposed basin in northwest China (Fig. 1b; Cao et al., 2015; Cao et al., 2020). During the late Paleozoic it was located within central Siberia at high northern latitudes (~40°N) (Fig. 1a; Sengor et al., 1993; Wan et al., 2010). The Junggar Basin is developed on Carboniferous basement and is a remnant lake basin of the southeastern marine regression (Gao et al., 2020). Mahu Sag is an extensional fault sag located in the northwest part of the basin (Fig. 1b). It contains late Paleozoic to Cenozoic terrestrial sediments and has experienced multiple stages of tectonic deformation; thus, these sedimentary sequences have recorded the long-term tectonic and paleoenvironmental evolution of the Kazakhstan Plate (Liu et al., 2017; Yu et al., 2018; Tang et al., 2021a).

During the late Paleozoic, sediments from the provenance near the central West Junggar accretionary orogen were continuously supplied to the basin, resulting in the development of the Fengcheng Fm (Tang et al., 2021a). Due to strong tectonic activity the depositional processes and stratigraphic correlation in Mahu Sag are unclear (Yu et al., 2018), and the exact chronostratigraphic attribution of the Fengcheng Fm remains controversial. The main part of the Fengcheng Fm comprises a continuous sequence of multi-source, fine-grained sediments deposited in an alkaline lake environment, including near-source clastic materials, chemical sediments, and peripheral volcanic materials (Guo et al., 2021; Tang et al., 2021b; Zhi et al., 2019). During the depositional period of the Fengcheng Fm, the runoff from the northern and western margins carried sediments into the sag and formed two deltas (Fig. 1c). The western delta is dominated by siliciclastic deposits, including sandy conglomerate, sandstone and siltstone, while the northern delta is mainly composed of volcanic materials (Wang et al., 2022). The center of the sag was mainly a semi-deep to deep lake environment, where thick shale and calcareous shale are the dominant lithologies and volcanic materials are less developed (Fig. 1c, 2a). In Well MY1, the bottom of the Fengcheng Fm contains multiple layers of basalt and tuff. The central part mainly comprises interbeds of shale and calcareous shale, with a high carbonate content and containing alkaline minerals. The top part is coarse-grained and the dominant lithologies are siltstone and sandstone (Fig. 2a). The Fengcheng Fm developed a set of delta-lacustrine deposits within a stable sedimentary environment without obvious seismic interruption of the sedimentation. Thus, this sedimentary sequence preserves a complete paleoclimatic and paleoenvironmental record of a late Paleozoic terrestrial high-latitude lake basin (Gao et al., 2020; Huang et al., 2021; Wang et al., 2022).

3. Methodology

3.1. Samples and stratigraphic data

Natural Gamma Ray (GR) logging has been widely used in astrochronological research (e.g., Falahatkhah et al., 2021; Jin et al., 2019; Wang et al., 2020a). Natural GR activity is determined by the sedimentary concentration of radioactive minerals (U, Th, K), which reflects variations in the mud and organic matter content. GR activity is generally higher in mudstones and lower in sandstones and carbonates. Variations in the mud and organic matter content may be driven by astronomically-forced climate change, and thus GR logging is widely regarded as providing valuable sedimentary information and is one of the most sensitive indicators for retrieving astronomically-forced climatic signals (Li et al., 2019a). Well MY1 is located within the sedimentary center of Mahu Sag; it was drilled through the entire Fengcheng Fm and contains a thick sedimentary sequence. A GR log for the depth interval of 4520–4860 m within the shale sediments of Well MY1 (Fig. 2a), covering the whole of the Fengcheng Fm, was used for astrochronological analysis (Fig. 2a). The stratigraphic resolution of the GR series is 0.125 m.

We collected 90 core samples from the Fengcheng Fm of Well MY1 for organic carbon isotope analysis which was conducted according to the China National Standard (GB/T 18340.2-2010). The sample depths ranged from 4577.67 m to 4754.8 m, with the average sampling interval of 1.99 m. The lithology of this interval is dominated by shale and calcareous shale. After grinding to pass a 200-mesh sieve, sample powders were heated in a water bath

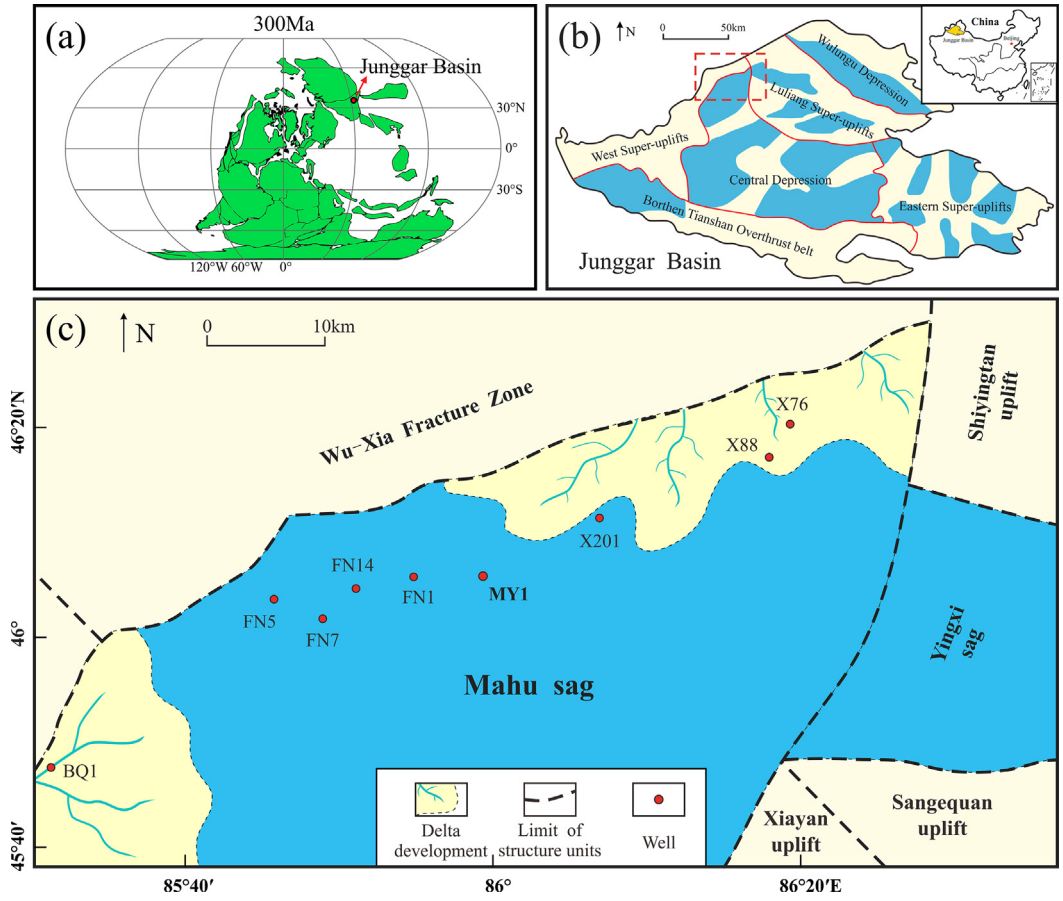

Fig. 1. Overview of the study area. (a) shows the location of Junggar basin at ca. 300 Ma Paleogeographic map. The base map is from https://portal.gplates.org/. (b) Location of Mahu sag in Junggar Basin. (c) Structural division of Mahu Sag and its periphery.

with 3 mol/L HCl to remove inorganic carbon, and then rinsed to neutrality for carbon isotope analysis. The carbon isotope composition was measured using a Thermo Scientific (thermoelectric) FLASH HT EA-MAT 253 IRMS, and the carbon isotopes were separated and determined by gas chromatography–mass spectrometry. The standard materials are IAEA-600 Caffeine and USG24 Graphite, and the results are expressed according to the Pee Dee Belemnite (PDB) standard. A parallel sample was added every 10 samples, and the uncertainty of the analysis was within 0.2 ‰. Sample pretreatment and analysis were conducted in the State Key Laboratory of Petroleum Resources and Prospecting, China University of Petroleum (Beijing).

3.2. Time series analysis

Periodic components in the GR log were detected using wavelet analysis (Torrence and Compo, 1998). Then, 80 m Locally Weighted Scatterplot Smoothing (LOESS) was conducted to remove the long-term trend (Fig. 2a). To determine the power of the periodic components, the 2π multi-taper method (MTM) was used to conduct power spectrum analysis (Thomson, 1982). Robust red noise analysis was conducted to identify any significant frequencies (Mann and Lees, 1996). The Correlation Coefficient (COCO) were applied to estimate the optimum sedimentation rate (Li et al., 2018a). According to the study of Huang et al. (2021) in Fengcheng Fm, the sedimentation rate evaluated by COCO ranging from 0.1 to 20 cm/Kyr with a step of 0.1 cm/Kyr, and 5000 Monte Carlo simulations were conducted. In order to validate the results of COCO, TimeOpt analysis was used to test sedimentation rates repeatedly (Meyers, 2015). The sedimentation rate test ranges from 5 to 20 cm/Kyr with a step of 0.1 cm/Kyr, and 5000Monte Carlo simulations were conducted. Evolutionary Fast Flourier Transform analysis was applied to characterize the temporal evolution of periodic components of the GR series (Kodama and Hinnov, 2015). A Gaussian filter was used to obtain the target astronomical cycle of the data series (Paillard et al., 1996), and the filter bandwidth set to 0.002469 ± 0.0002 (long eccentricity), 0.0064 ∼ 0.0126 (short eccentricity), 0.0282 ± 0.0056 (obliquity) and 0.0524 ± 0.0155 (precession). The above numerical analyses were performed using Acycle 2.3 software (Li et al., 2019b).

3.3. Astronomical parameters for the early Permian (∼300 Ma)

The current astronomical solution only covers the Mesozoic (0–249 Ma), and no comprehensive astronomical solution has been proposed beyond 250 Ma (Fang et al., 2017). However, due to Jupiter's stable orbit and huge mass, the 405-kyr-long eccentricity period is stable over most of geological time (Laskar et al., 2004, 2011). Thus, the long and short eccentricity cycles were determined using the La2004 orbital solution (Laskar et al., 2004). The target obliquity and precession periods and their uncertainties at 300 Ma were estimated according to Waltham (2015). The parameters show that the theoretical ratios of the long eccentricity, short eccentricity, obliquity, and precession cycles are approximately 21:6:1.8:1 at 300 Ma (Table 1).

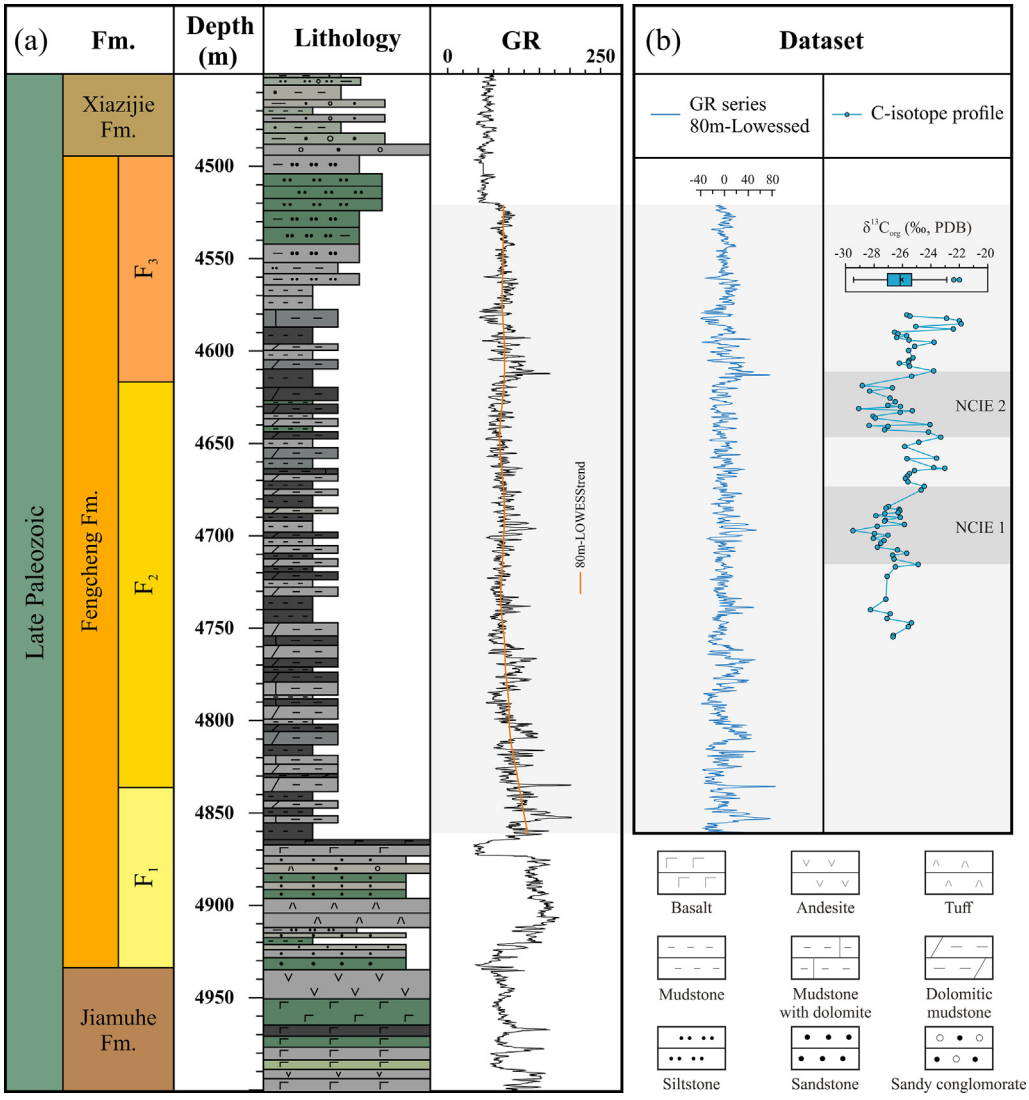

Fig. 2. Stratigraphy, lithology, and data series of well MY1. (a) Stratigraphy, lithology, and original gamma ray (GR) series. The sudden change at 4520 m of the GR series derive from the twice measurements of the upper-part and lower-part data. (b) Detrended GR series and organic carbon isotope series. The orange line is the 80 m 'Lowess' trend. (For interpretation of the references to colour in this figure legend, the reader is referred to the web version of this article.)

Table 1
Astronomical parameters at 300 Ma and cyclicities in GR series.

Term	Target periodicity (kyr) (By Laskar et al., 2004; Waltham, 2015)	GR series cyclicity in depth domain (m)	GR series cyclicity in time domain (kyr)
Long eccentricity	405	40.48	405
Short eccentricity	125	11.49	117
	95		
Obliquity	35.5 ± 2.9	3.59	37.2
Precession	21.7 ± 1.1	2.07	22.4
	20.6 ± 0.97		
	17.8 ± 0.77		17.4
	17.66 ± 0.76		16.4
Ratio	21: 6: 1.8: 1	21: 6: 1.9: 1.1	
Sedimentation rate (cm/kyr)	/	10	

4. Results

4.1. Organic carbon isotopes

The organic matter in the Fengcheng Fm is mainly type II_2 (Jiang et al., 2022), indicating that the source is mainly primary producers such as bacteria and algae, with additional contributions from pollen and the detritus of terrestrial plants (Cao et al., 2020; Guo et al., 2021). Photosynthetic carbon sequestration by primary producers can reflect changes in the carbon cycle (Hayes et al., 1999; Kump and Arthur, 1999). Thus, stratigraphic changes in $\delta^{13}C_{org}$ within the Fengcheng Fm may reflect changes in the environment,

including the biota. The $\delta^{13}C_{org}$ record shows frequent changes within the range of −27.87 ‰ to −29.48 ‰ (Fig. 2b). Two negative carbon isotope excursions (NCIEs) are evident in the profile. NCIE 1 is within the depth interval of 4697–4708 m, with the initial value of −26.36 ‰ and amplitude of 3.12 ‰. The amplitude of NCIE 1 is larger than that of NCIE 2 and it corresponds to the minimum value within the entire $\delta^{13}C_{org}$ profile. NCIE 2 is within the depth interval of 4621–4644 m, within which $\delta^{13}C_{org}$ decreases gradually, with frequent fluctuations superimposed, from the initial value of −25.3 ‰ before attaining the final value of −28.1 ‰.

4.2. Astrochronological analysis

The wavelet transform shows a continuous ~ 40 m periodicity throughout the GR record (Fig. 3b), implying a relatively uniform sedimentation rate. In addition, the power spectrum analysis results indicate multiple spectral peaks that exceed the 95 % confidence level (Fig. 3c); these dominant peaks have the following wavelengths (in meters): 40.48, 14.93, 11.49, 3.59, 2.07 and 1.56, and they correspond to the signals identified in the wavelet transform.

The results of COCO analysis reveal the strongest correlation from 9.6 to 10.1 cm/kyr, with a significance level < 0.01 for the null hypothesis (Fig. 3d; H_0: no astronomical forcing). The TimeOpt result indicates that the optimum sedimentation rate is 9.9 cm/kyr (Fig. 3e). The agreement between the COCO and TimeOpt results suggests that the sedimentation rate of the GR series is ~ 10 cm/kyr, which agrees with the results of Huang et al. (2021). Consequently, the 40.48 m wavelength peak most likely represents the 405-kyr long eccentricity signal. In the GR series, the wavelength ratios of 40.48, 11.49 m, 3.59 m, and 2.07 m are 21:6:1.9:1.1, respectively, which is in excellent agreement with the target astronomical ratios for 300 Ma (Table 1). These results are convincing evidence for the presence of Milankovitch cycles in the sedimentary record of the Fengcheng Fm.

The 405-kyr long eccentricity cycle is regarded as the most stable astronomical cycle in the Phanerozoic and hence it can be used as a 'metronome' to establish a time scale for Phanerozoic strata (Laskar et al., 2004, 2011). Based on the interpretation of the average sedimentation rate and astronomical cycles, the frequency component centered at 1/40.48 m^{-1} was extracted using a Gaussian band-pass filter. This signal was then calibrated to the 405-kyr long eccentricity cycle. The power spectrum of the calibrated GR series provides strong evidence of astronomical cycles with periodicities of 405 kyr, 117 kyr (short eccentricity), 37.2 kyr (obliquity), and 22.4 kyr, 17.4 kyr, and 16.4 kyr (precession) (Fig. 4c). The evolutionary Fast Fourier Transform results show that periodic signals are continuous within the time domain (Fig. 4c).

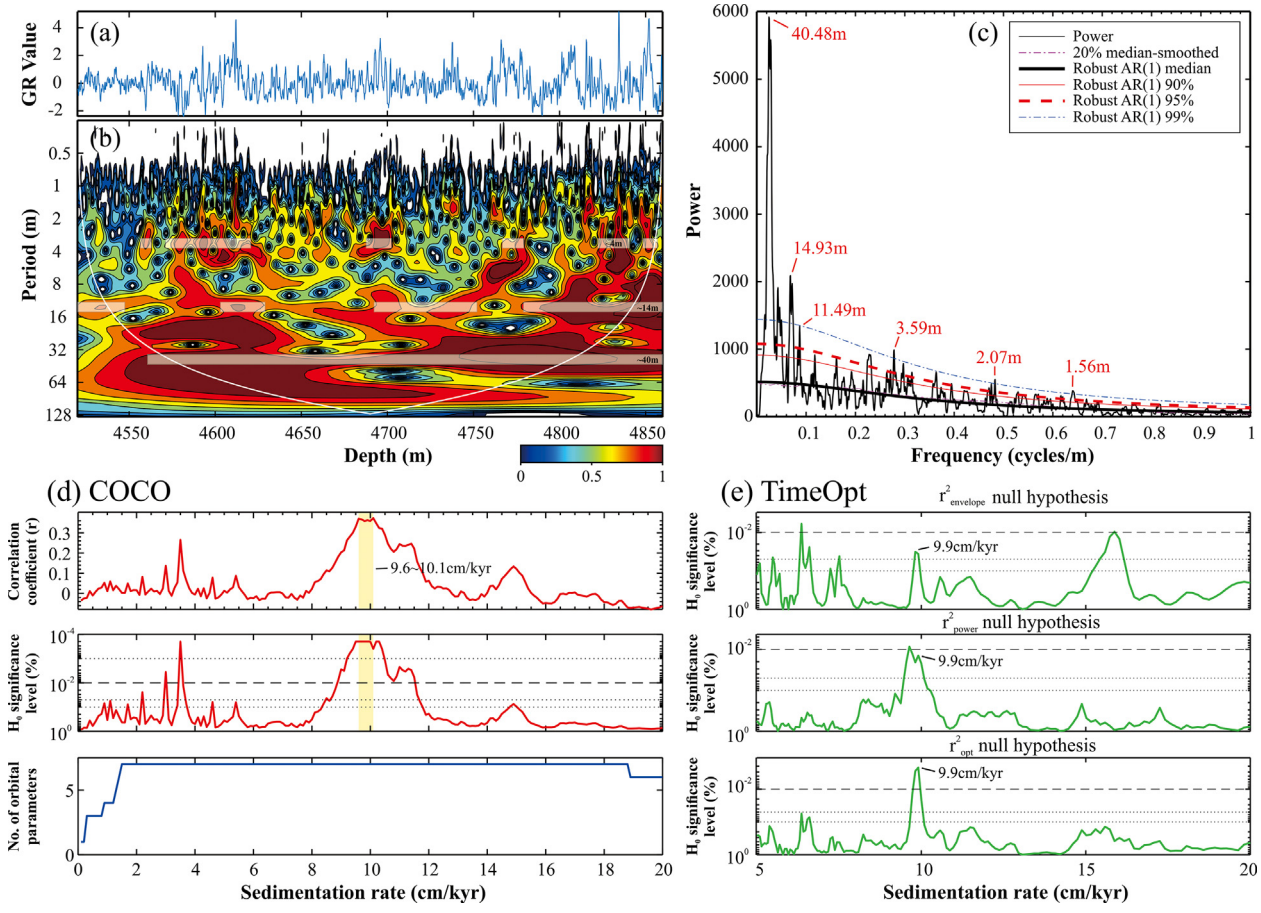

Fig. 3. (a) Detrended GR series. (b) Wavelet transform of GR series. The white shaded area shows cyclicities with wavelengths of ~ 40 m, ~14 m and ~ 4 m. Edge effects become apparent in the area outside of the white line. (c) 2π MTM power spectra of selected GR series. Robust AR (1) model and different confidence levels show the significant peaks, which are marked with the inverse of frequency. (d) COCO analysis: Correlation coefficient (upper), null hypothesis and H_0 significance level (middle; H_0: no astronomical forcing), and number of contributing astronomical parameters (bottom). The sedimentation rate test from 0.1 to 20 cm/kyr with steps of 0.1 cm/kyr. (e) TimeOpt analysis: Pearson correlation coefficient for the precession amplitude envelope fit ($r^2_{envelope}$), spectral power fit (r^2_{power}), and combined envelope and spectral power fit (r^2_{opt}). H_0: no astronomical forcing. The sedimentation rate tested from 5 to 20 cm/kyr with a test step of 0.1 cm/kyr. The Monte Carlo simulations number of both COCO and TimeOpt were 5000. In Fig. 3d and e, the grey dotted and dashed lines from bottom to top are 90 %, 95 %, 99 %, 99.9 % confidence level, respectively. For highlight, we denote 95 % confidence level by dashed line.

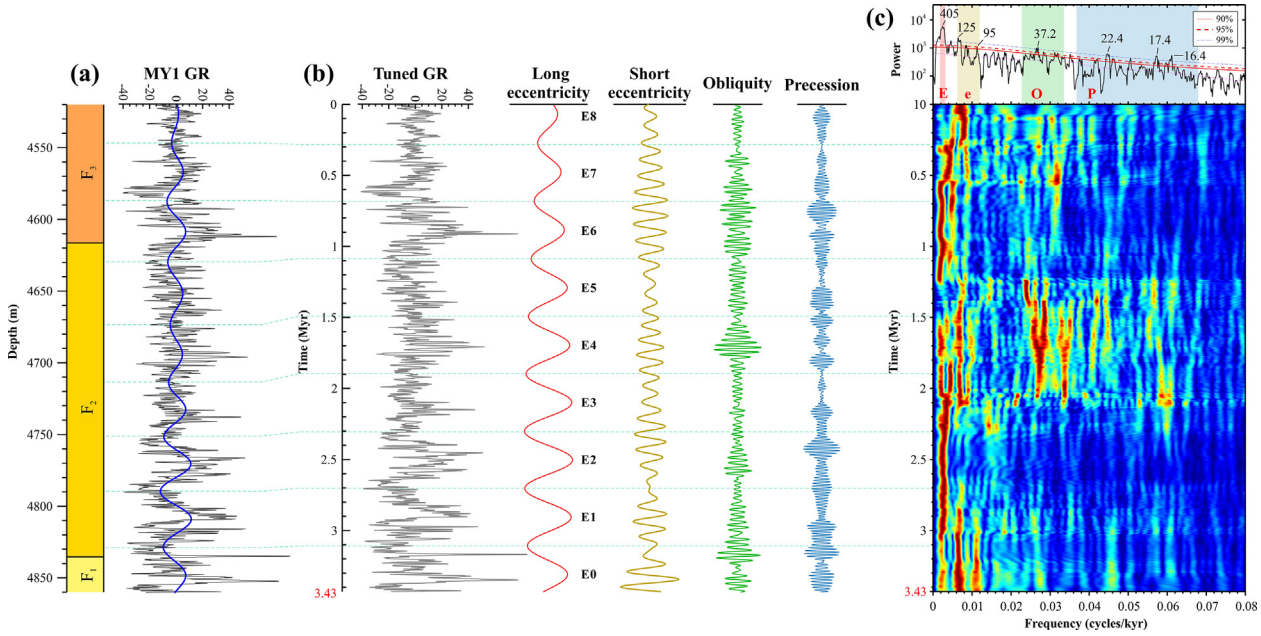

Fig. 4. Astronomical time scale of selected GR series of MY1. (a) Selected GR series in depth domain. (b) GR series in time domain and the cycles of long eccentricity (red), short eccentricity (yellow), obliquity (green), and precession (blue). (c) 2π MTM power spectra and evolution fast Fourier transform (FFT, 650kyr sliding window) of selected GR series in time domain. The shaded area shows the filter bandwidth of long eccentricity (0.002469 ± 0.0002), short eccentricity (0.0064 ∼ 0.0126), obliquity (0.0282 ± 0.0056), and precession (0.0524 ± 0.0155). (For interpretation of the references to colour in this figure legend, the reader is referred to the web version of this article.)

The spectral signal characteristics match those of the theoretical astronomical period (Waltham, 2015; Table 1), which further supports our interpretation of the astronomical forcing of sedimentation. Consequently, we were able to obtain a floating astronomical time scale (ATS) for the studied stratigraphic interval using the 405-kyr calibration result (Fig. 4a). This floating time scale reveals nine long eccentricity cycles within the depth interval of 4520–4860 m, with the duration of ∼ 3.43 Myr. The late Paleozoic astronomical cycles were established via depth-time tuning of the 405-kyr long eccentricity cycle (Fig. 4b). The results of power spectrum analysis in the time domain suggest that the following periodic components are recorded in the Fengcheng Fm: the short eccentricity period (∼117 kyr), obliquity (37.2 kyr), and the precession periods of 22.4 kyr, 17.4 kyr, and 16.4 kyr (Fig. 4c, Table 1).

5. Discussion

5.1. Age constraints

Multiple zircon U-Pb dating studies have been conducted on the Late Paleozoic strata in Mahu Sag (Liu et al., 2019; Wang et al., 2020b; Wang et al., 2022). The U-Pb chronology of Well X201, close to Well MY1, was used to fix our floating time scale (Fig. 5, green point; Wang et al., 2022). Well X201 is close to the northern delta which is composed of an extensive set of tuff, basalt and tuffaceous clastic rocks. However, it is difficult to achieve a complete lithological correlation between wells X201 and MY1, and therefore in this study we used the combination of GR logging curve characteristics combined with the lithology and grain size to align the two wells. Under the constraint of sub-member boundaries, we observed three typical features in the GR log for Well X201 within the depth interval of 4863–4890 m, which are correlative with the depth interval of 4840–4910 m in GR log for Well MY1 (Fig. 5a, b). Moreover, these intervals have similar lithological and grain-size characteristics: finer-tuff-coarser-mud. Consequently, we consider that the depth intervals of 4926–4944 m in Well X201 and 4895.69–4911.36 in Well MY1 contain the same tuff layer (Fig. 5a, b). Based on the alignment of this layer, the age anchor for Well MY1 was fixed at the boundary of the tuff layer (4895.69 m). The basalt layer above this anchor was formed by a brief eruption and its effect on the floating time scale needs to be removed (Fig. 5b, blue dashed line). The age anchor is located 23.14 m below the basalt, and the spacing is roughly estimated to be half the thickness of a 405 kyr cycle. Consequently, the position of the age anchor in the time domain was determined, which in turn fixed the floating time scale (Fig. 5c). The ATS contains nine long eccentricity cycles within the depth interval of 4520–4860 m of the Fengcheng Fm in Well MY1, with the duration of 300.59–297.16 Ma (±1.3 Myr). The uncertainty is derived from the error bar of the zircon U-Pb age and the inaccuracy of the age anchor position in Well MY1, where the former is much larger than the latter.

5.2. Astronomical constraint on the Carboniferous-Permian Boundary

The CPB is defined as the conodont first appearance datum of the isolated-nodular morphotype of *Streptognathodus "wabaunsensis"* (Aretz et al., 2020; Cohen et al., 2021; Davydov et al., 1998). Previous attempts to constrain the CPB were based mainly on biostratigraphic and radioisotope ages. Dunn (2001) conducted a systematic study of the biostratigraphy of the Aidaralash Creek stratotype in northern Kazakhstan, and characterized the biological context of the CPB. Ramezani et al. (2007) obtained numerous high-precision U-Pb zircon ages that constrained the position and age of the CPB in the southern Urals (298.9 ± 0.4 Ma), and the latest GTS2020 time scale reduced the age error (298.9 ± 0.15 Ma; Aretz et al., 2020). Michel et al. (2015) revised the chronostratigraphy of the Lodève Basin, in southern France, based on U-Pb zircon ages of tuff beds and constrained the age of the CPB. Previous studies in the Junggar Basin have tended to define the unconformity between the marine basement and the terrestrial Jiamuhe Fm as the CPB (e.g., Buckman et al., 2004; He et al., 2018). However, several recent

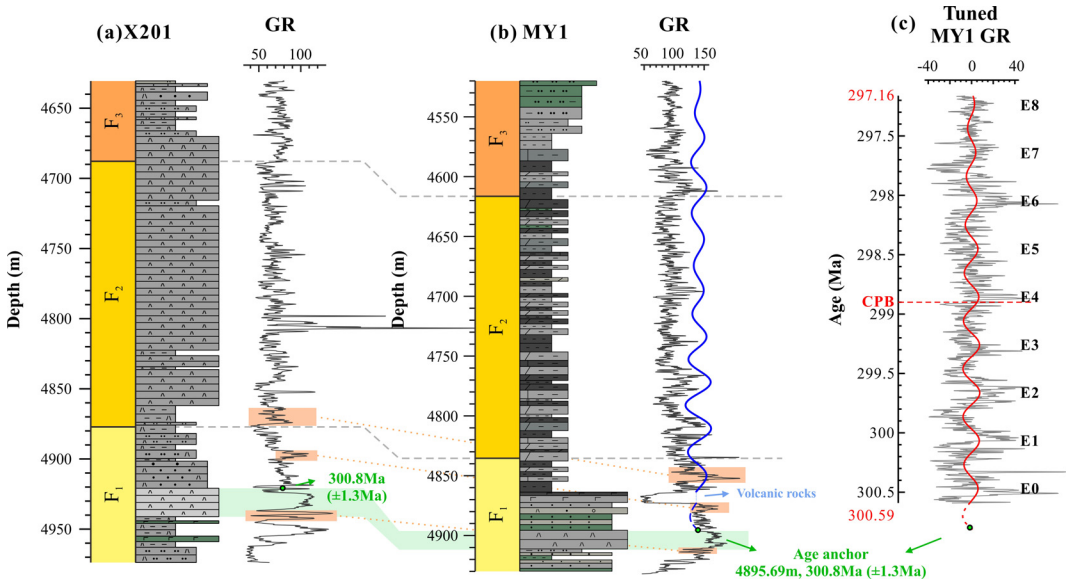

Fig. 5. (a) X201 lithology and GR series. (b) MY1 lithology, GR series, and its ~ 40.48 m cycle which filtered with 0.0247 ± 0.0049 passband. (c) 405kyr long eccentricity cycles of MY1 GR series in time domain. The green point is the zircon U-Pb age from Wang et al., (2022). The orange shaded areas connected by dashed lines showing the similar GR curve features in the two wells used to calibration the age anchor position. The green shaded area showing the marker layer with the same lithology. (For interpretation of the references to colour in this figure legend, the reader is referred to the web version of this article.)

studies have suggested that the CPB is located within the continuous sequence of deposits overlying the unconformity (e.g., Gao et al., 2020; Huang et al., 2021). Wang et al. (2022) reported that the depositional age of the Fengcheng Fm was ~ 300 Ma, implying it was the first stratum deposited after the Carboniferous. The present study provides a more precise chronological constraint on the CPB in the Junggar Basin and it revises the chronostratigraphic attribution of the Fengcheng Fm. The ATS constrains the Fengcheng Fm to the Gzhelian–Asselian, and preliminarily constrains the CPB to the depth of 4698.83 m in Well MY1. The deposits of the Fengcheng Fm straddle the CPB and provide a valuable record of climate change across the Carboniferous–Permian transition (Fig. 5).

5.3. Carbon isotope responses at the Carboniferous-Permian Boundary

Several carbonate platforms in China, such as the Yangtze platform (e.g., the Kongshan and Zhongdian profiles) contain a NCIE at the transition between the Gzhelian and Asseian (e.g., the Kongshan profile, Fig. 6d; Buggisch et al., 2011). These NCIEs were interpreted as the effect of meteoric diagenetic alteration on the exposed carbonate platforms caused by a maximum in ice sheet extent and sea-level decrease (Aretz et al., 2020; Buggisch et al., 2011). However, several studies have suggested that the global climate warmed and that glaciers melted in the late Gzhelian, while in the early Asselian the climate cooled and the Gondwana Glacier expanded, causing global sea-level regression (Durante, 1995; Phillips and Peppers, 1984; Montañez and Poulsen, 2013). However, this is inconsistent with the foregoing diagenetic explanation. In contrast, Haq and Schutter (2008) suggested that the global sea level was at a high level during the transition between the Carboniferous and Permian. The Naqing succession in south China, which is considered to have been deposited within a deep-ocean carbonate environment, also shows a sharp NCIE (Fig. 6e, Buggisch et al., 2011). It has been attributed to the effect of sea-level changes on deep ocean circulation, which in turn altered the $\delta^{13}C$ of the deep ocean. Consequently, the NCIE in the carbonate platforms of south China may not have been the result of changes in sub-aerial diagenesis and further research is needed to confirm their origin.

A similar negative carbon excursion has been observed in terrestrial carbon isotope profiles, implying that the NCIE may be of global extent. Lu et al. (2021) reported a $\delta^{13}C_{org}$ NCIE from the Gzhelian to Asselian in the terrestrial Shimenzhai profile (Fig. 6c). The NCIE is interpreted to represent a change in the isotopic composition of atmospheric CO_2 caused by the combined effects of the movement of the North China Plate, Tarim Plate volcanism, and the Skagerrak-Centered Large Igneous Province. The $\delta^{13}C_{org}$ profile of Well MY1 in the Fengcheng Fm also records a NCIE close to the CPB, identified by the ATS (Fig. 6b, NCIE 1), and Wang et al. (2022) reported a similar NCIE in an integrated $\delta^{13}C_{carb}$ profile of the Fengcheng Fm (Fig. 6a). There is no correlation between the carbon and oxygen isotope records in the Fengcheng Fm (Wang et al., 2022), which suggests that the carbon isotope profile is a primary signal of the carbon cycle with minimal diagenetic modification. Photosynthetic carbon sequestration by primary producers would preferentially fix atmospheric ^{12}C, resulting in carbon isotope fractionation (Hayes et al., 1999; Kump and Arthur, 1999). The organic matter of the Fengcheng Fm is mainly type II_2, which is derived from a mixture of aquatic algae and terrestrial plants, and the carbon isotope record reflects changes in atmospheric CO_2 composition (Jiang et al., 2022; Ding et al., 2017). Thermal degradation of organic matter can lead to a decrease in the total organic carbon content, causing an enrichment of the $\delta^{13}C$ of the residual organic carbon (Hayes et al., 1999); however, this process would not affect the trends of $\delta^{13}C_{org}$ records (Des et al., 1992). Although differences in timing and magnitude may exist, the $\delta^{13}C_{org}$ and $\delta^{13}C_{carb}$ excursions in the Fengcheng Fm appear to record the same event. After compiling all the $\delta^{13}C_{org}$ profiles, the existence of a global NCIE from the Gzhelian to the Asselian was confirmed, which is characterized by a continuous negative excursion following a brief positive excursion, after which the $\delta^{13}C$ composition became heavier. This NCIE is reliable evidence for constraining the position of the CPB. The coupled negative excursions of $\delta^{13}C_{carb}$ and $\delta^{13}C_{org}$ may represent a change in the isotopic composition of atmospheric CO_2. Thus, NCIE 1 is likely to be the result of volcanic activity releasing mantle-derived CO_2 into the atmosphere, which is consistent with the interpretation of Lu et al. (2021). Our ATS-based estimate of the

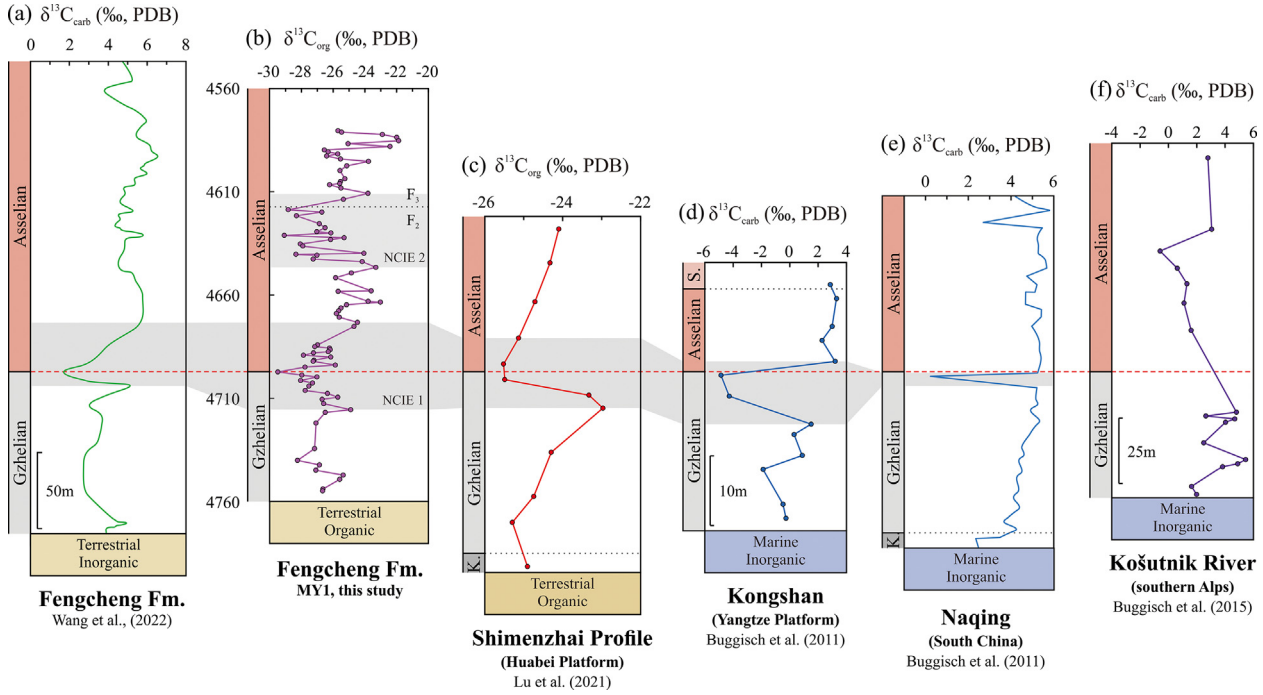

Fig. 6. Global comparison of $\delta^{13}C$ profiles. (a) $\delta^{13}C_{carb}$ profile of Fengcheng Fm, modified from Wang et al. (2022). (b) $\delta^{13}C_{org}$ profile of Fengcheng Fm in MY1, this study. (c) Terrestrial $\delta^{13}C_{org}$ of Shimenzhai profile, Huabei Platform, modified from Lu et al. (2021). (d) Marine $\delta^{13}C_{carb}$ of Kongshan profile, Yangtze Platform, modified from Buggisch et al. (2011). (e) Marine $\delta^{13}C_{carb}$ of Naqing succession, South China, modified from Buggisch et al. (2011). (f) Košutnik River, Southern Alps, modified from Buggisch et al. (2015). K. Kasimovian; S. Sakmarian. The grey area shows the global correlation of NCIE1.

duration of NCIE 1 is 425.23 kyr, representing the impact of volcanic activity on the carbon cycle.

Although ocean–atmosphere interactions link the terrestrial and marine carbon cycles, the corresponding carbon isotope signals can be substantially different depending on various factors (Diefendorf and Freimuth, 2017; Nordt et al., 2016). In some studies, the carbon isotopic composition organic carbon and terrestrial plant biomarkers has been shown to vary between rainy and dry seasons (Marwick et al., 2014; Ponton et al., 2014). This appears that the fractionation of $\delta^{13}C_{org}$ in these regions are mainly regulated by local water availability, while the influence of global pCO_2 seems less significant. During plant carbonization caused by wildfire events, the cellulose degrades earlier than lignin in wood, which results in a decrease in the overall $\delta^{13}C$ value (Czimczik et al., 2002). The thermal metamorphic stage of Coalification during diagenesis can lead to an increase the $\delta^{13}C$ composition of decaying plants by about 0.5 ‰ (Fang et al., 2014). In Fengcheng Fm, Changes in the source of the organic matter may have a limited effect on the $\delta^{13}C_{org}$ record of the Fengcheng Fm. This negative carbon isotope excursion has the consistent amplitude of ~ 5 ‰ in the Fengcheng Fm, Kongshan succession, and Naqing succession. However, the amplitude of this excursion in the Shimenzhai profile is smaller (3 ‰), which may be the result of various local factors affecting organic carbon burial. In addition, an inadequate sampling density would lead to a low-resolution or degraded $\delta^{13}C$ signal (Fig. 6c, d, f), increasing the difficulty of global correlation. Hence, higher resolution C-isotope profiles are needed to further investigate the NCIE.

5.4. Constraining the Carboniferous–Permian Boundary in Well MY1

In this study of Well MY1 in the Fengcheng Fm we have constrained the CPB to the depth of 4698.83 m, and assigned an absolute age using our ATS, while the depth of 4697.28 m is indicated by the carbon isotope stratigraphy. The depth offset of these two estimates is 1.55 m (Fig. 7). And determining the exact position of the CPB in the Junggar Basin requires further investigation. The uncertainty of the stratigraphic position of the CPB is the result of three factors: the astronomical time scale, the age anchor, and the NCIE.

Astronomical cycles have been shown to influence Earth's climate via their control on ice sheet expansion and contraction, eustatic fluctuations, land–ocean water exchange, and the migration of climate zones (Li et al., 2018b; Lisiecki and Raymo, 2005; Liu et al., 2015; Wang et al., 2004). The origin of the astronomical signal in the GR series of the Fengcheng Fm likely to be the astronomical forcing of shifts in climatic zones, which led to periodic changes in regional monsoon intensity and runoff to the Junggar Basin, which turn controlled the input of clay minerals. Ice sheets are a potential amplifier of the astronomical forcing of climate change at high latitudes, resulting in a more prominent astronomical signal in the GR record (Fang et al., 2017). The low H_0 significance level in the COCO results and the agreement between the sedimentation rate estimated in this study with that of Huang et al. (2021) indicate that astronomical signals are accurately preserved within the GR log of Well MY1.

The age anchor is based on the U-Pb age of tuff at the depth of 4923.7 m in Well X201 (Wang et al., 2022). The U-Pb age is derived from 32 zircon grains, almost all of which were euhedral and semi-euhedral crystals with obvious oscillating rings, indicating their magmatic origin. These features demonstrate the reliability of this U-Pb age. The anchor was precisely transferred from Well X201 to Well MY1 based on the comparison of the subdivision boundaries of the Fengcheng Fm, the GR logs, and the lithological boundaries of the two wells. Based on the U-Pb age and its uncertainty, and the time-depth conversion relationship, the CPB was constrained to the depth range of 4563.5–4821.9 m (Fig. 7).

Two NCIEs are evident in the $\delta^{13}C_{org}$ profile within the above-mentioned interval (Fig. 7c). NCIE 1 has the same characteristics as those of previously reported profiles and is consistent with the

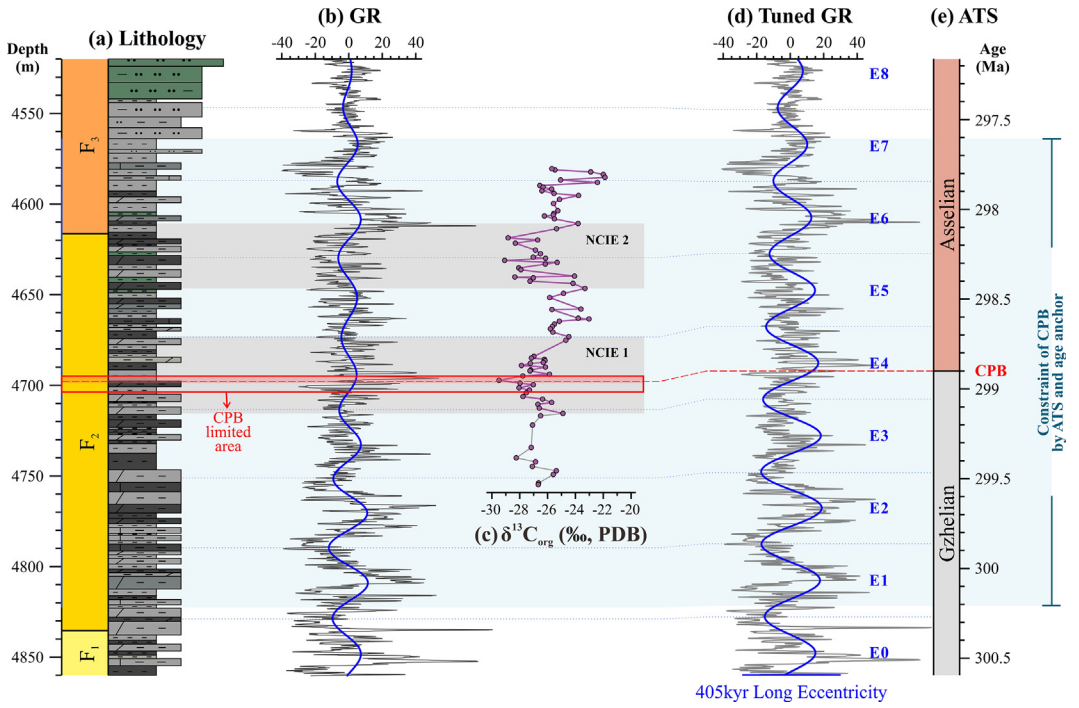

Fig. 7. Limitation of CPB. (a) Lithology of study interval, MY1. (b) GR series and its ~ 40.48 m cycle (blue line). (c) $\delta^{13}C_{org}$ profile. The 2 grey shaded area shows the NCIEs. (d) Tuned GR series and its 405kyr long eccentricity cycle. (e) Astronomical Time Scale. The cyan shaded area shows the constraint of CPB by ATS and U-Pb age and its uncertain. The red shaded area shows the floating limit of CPB by $\delta^{13}C_{org}$ sampling rate. The red box shows the finally limited area of CPB identified by the carbon burial lag uncertainty in lakes and the floating limit. The red line suggests the temporary CPB position (4698.83 m) determined by ATS. (For interpretation of the references to colour in this figure legend, the reader is referred to the web version of this article.)

$\delta^{13}C_{carb}$ profile (Fig. 6). NCIE 2 has frequent fluctuations with numerous single sample negative excursions, indicating that the event was likely caused by changes in the source of sedimentary organic matter. Within the depth interval of 4563.5–4821.9 m the probability of the presence of the CPB at each depth follows a normal distribution, which is the same as that of the U-Pb age uncertainty. Probabilistically, NCIE 1 is more likely to be the NCIE corresponding to the CPB. In NCIE 1, the upper and lower sampling depths of the maximum negative excursion point are 4694.84 m and 4698.82 m, respectively, constraining the CPB to float within the range of 3.98 m. Previous studies have found that paleoclimate proxies have different responses and sensitivities to astronomical forcing (Li et al., 2019b; Ma and Li, 2020). Based on a study of Oligocene deep-sea deposits, Zachos et al. (2001) found a lag between astronomical forcing and ocean carbon burial. Compared with the theoretical astronomical period (La2004 time scale), the 405-kyr periodicity extracted from the deep-sea carbon isotope record has the phase lag of ~ 10 %–15 %, which may be attributed to the long residence time of carbon in the ocean (~10^5 yr). The relatively uniform lithology during NCIE 1 implies a stable lacustrine environment and a uniform carbon burial process. In such a lake environment, a similar lag should exist in lake carbon burial. Here, we assign the maximum uncertainty of 50 kyr based on the maximum ocean carbon burial lag. Considering the carbon burial lag effect in lakes and the floating limit of the CPB, we finally constrained the CPB in Well MY1 to the depth range of 4694.84–4703.56 m (Fig. 7). The CPB delimited by the ATS (4698.83 m) was taken as a preliminary estimate.

6. Conclusions

In this study of the Late Paleozoic Fengcheng Fm in the Junggar Basin we have determined the response of terrestrial carbon isotopes to the Carboniferous–Permian Boundary, which confirms the global synchrony of this response. Our results provide new evidence for the stratigraphic delimitation of the Carboniferous–Permian Boundary in terrestrial environments, and they provide a basis for subsequent stratigraphic correlation and comparison. Our main conclusions are as follows:

(1) The high-resolution astronomical time scale indicates nine 405-kyr long eccentricity cycles within the depth interval of 4520–4860 m in Well MY1 of the Fengcheng Fm, with the duration of 300.59–297.16 Ma (±1.3 Ma). This new chronostratigraphic frame constrains the Fengcheng Fm to the Gzhelian–Asselian and provides a revised chronostratigraphic attribution of the terrestrial strata in the Junggar Basin. The Carboniferous-Permian Boundary is confirmed to exist in the Fengcheng Fm deposits.

(2) Comparison of carbon isotope profiles revealed a negative carbon isotope excursion at the transition between the Gzhelian and Asselian, characterized by a continuous negative excursion following a short positive excursion, after which the $\delta^{13}C$ composition became heavier. This event is evident in both the $\delta^{13}C_{org}$ and $\delta^{13}C_{carb}$ profiles and it has the duration of 425.23 kyr. This event represents a change in the atmospheric CO_2 isotope composition and it can be used to delimit the CPB.

(3) The accuracy of the astronomical time scale, the age anchor, and the NCIE are verified, allowing the position of the CPB in MY1 to be determined. Based on the sampling interval of the $\delta^{13}C_{carb}$ profile, the CPB was determined to be floating within the depth interval 3.98 m. A maximum uncertainty of 50 kyr was assigned based on the lag in ocean carbon burial. Based on the various uncertainties, the CPB is constrained to the depth interval of 4694.84–4703.56 m in Well MY1, and its position as determined by ATS (4698.83 m) is taken as a preliminary estimate.

CRediT authorship contribution statement

Renda Huang: Software, Methodology, Formal analysis, Visualization, Writing - original draft, Writing - review & editing. **Fujie Jiang:** Conceptualization, Supervision, Writing - review & editing. **Di Chen:** Visualization, Supervision, Writing - review & editing. **Ruoyuan Qiu:** Validation, Writing - review & editing. **Tao Hu:** Supervision, Writing - review & editing. **Linhao Fang:** Supervision, Writing - review & editing. **Meiling Hu:** Investigation, Data curation. **Guanyun Wu:** Visualization, Data curation. **Chenxi Zhang:** Investigation. **Jiahao Lv:** Validation, Visualization. **Yuping Wu:** Investigation, Validation. **Liliang Huang:** Data curation, investigation.

Declaration of Competing Interest

The authors declare that they have no known competing financial interests or personal relationships that could have appeared to influence the work reported in this paper.

Acknowledgments

This study is supported by the National Natural Science Foundation of China (No. 41872128), the Strategic Cooperation Technology Projects of CNPC and CUPB (ZLZX2020-01-05), the Science Foundation of China University of Petroleum, Beijing (No. 2462020YXZZ021). We are grateful to the Xinjiang Oilfield for the support and help with experiments and basic data.

References

Aretz, M., Herbig, H.G., Wang, X.D., Gradstein, F.M., Agterberg, F.P., Ogg, J.G., 2020. Chapter 23 - The Carboniferous Period. In: Gradstein, F.M., Ogg, J.G., Schmitz, M. D., Ogg, G.M. (Eds.), Geologic Time Scale 2020. Elsevier, pp. 811–874.

Buckman, S., Aitchison, J.C., Malpas, J., Fletcher, C.J.N., Ali, J.R., Aitchison, J.C., 2004. Tectonic evolution of Palaeozoic terranes in West Junggar, Xinjiang, NW China. Geo. Soc. Special Pub. 226, 101–129.

Buggisch, W., Wang, X., Alekseev, A.S., Joachimski, M.M., 2011. Carboniferous-Permian carbon isotope stratigraphy of successions from China (Yangtze platform), USA (Kansas) and Russia (Moscow Basin and Urals). Palaeogeogr. Palaeoclimatol. Palaeoecol. 301, 18–38.

Buggisch, W., Krainer, K., Schaffhauser, M., Joachimski, M., Korte, C., 2015. Late Carboniferous to Late Permian carbon isotope stratigraphy: A new record from post-Variscan carbonates from the Southern Alps (Austria and Italy). Palaeogeogr. Palaeoclimatol. Palaeoecol. 433, 174–190.

Cao, J., Lei, D., Li, Y., Tang, Y., Abramiti, Chang, Q., Wang, T., 2015. High-quality source rocks of ancient alkaline lakes: Lower Permian Fengcheng Formation in Junggar Basin. Acta Petrol. Sinica 36, 781-790.

Cao, J., Xia, L., Wang, T., Zhi, D., Tang, Y., Li, W., 2020. An alkaline lake in the Late Paleozoic Ice Age (LPIA): A review and new insights into paleoenvironment and petroleum geology. Earth Sci. Rev. 202, 103091.

Cohen, K.M., Harper, D.A.T., Gibbard, P.L., 2021. ICS International Chronostratigraphic Chart 2021/10. International Commission on Stratigraphy. IUGS. www.stratigraphy.org (visited: 2021/12/23).

Czimczik, C.I., Preston, C.M., Schmidt, M.W.I., Werner, R.A., Schulze, E., 2002. Effects of charring on mass, organic carbon, and stable carbon isotope composition of wood. Org. Geochem. 33, 1207–1223.

Davydov, V.I., Glenister, B.F., Spinosa, C., Snyder, W.S., Ritter, S.M., Chernykh, V.V., Wardlaw, B.R., 1998. Proposal of Aidaralash as Global Stratotype Section and Point (GSSP) for base of the Permian System. Episodes 21, 11–18.

De Vleeschouwer, D., Da Silva, A.C., Sinnesael, M., Chen, D., Day, J.E., Whalen, M.T., Guo, Z., Claeys, P., 2017. Timing and pacing of the Late Devonian mass extinction event regulated by eccentricity and obliquity. Nat. Commu. 8, 2268.

Des, M.D., Strauss, H., Summons, R., Hayes, J., 1992. Carbon isotope evidence for the stepwise oxidation of the Proterozoic environment. Nature 359, 605–609.

Diefendorf, A.F., Freimuth, E.J., 2017. Extracting the most from terrestrial plant-derived n-alkyl lipids and their carbon isotopes from the sedimentary record: A review. Org. Geochem. 103, 1–21.

Ding, X., Gao, C., Zha, M., Chen, H., Su, Y., 2017. Depositional environment and factors controlling β-carotane accumulation: A case study from the Jimsar Sag, Junggar Basin, northwestern China. Palaeogeogr. Palaeoclimatol. Palaeoecol. 485, 833–842.

Dunn, M.T., 2001. Palynology of the Carboniferous-Permian boundary stratotype, Aidaralash Creek, Kazakhstan. Rev. Palaeobot. Palyno. 116, 175–194.

Durante, M.V., 1995. Reconstruction of Late Paleozoic climatic changes in Angaraland according to phytogeographic data. Stratigr. Geol. Correl. 3, 123–133.

Falahatkhah, O., Kadkhodaie, A., Ciabeghodsi, A.A., Wood, D.A., 2021. Astronomical forcing variations of the Upper Dalan Member (Late Permian) in the South Pars gas field, Persian Gulf, Iran. J. Asian Earth Sci. 209, 104689.

Fang, L., Lu, Y., Deng, S., 2014. Why Terrestrial Stable Carbon-isotope Stratigraphy Works: a Review. Acta Geol. Sin. – Engl. 88, 1603–1613.

Fang, Q., Wu, H., Hinnov, L.A., Jing, X., Wang, X., Yang, T., Li, H., Zhang, S., 2017. Astronomical cycles of Middle Permian Maokou Formation in South China and their implications for sequence stratigraphy and paleoclimate. Palaeogeogr. Palaeoclimatol. Palaeoecol. 474, 130–139.

Fielding, C.R., Frank, T.D., Birgenheier, L.P., Rygel, M.C., Jones, A.T., Roberts, J., 2008. Stratigraphic imprint of the late Palaeozoic ice age in eastern Australia; a record of alternating glacial and nonglacial climate regime. J. Geol. Soc. London 165, 129–140.

Gao, Y., Huang, H., Tao, H., Carroll, A.R., Qin, J., Chen, J., Yuan, X., Wang, C., 2020. Paleoenvironmental setting, mechanism and consequence of massive organic carbon burial in the Permian Junggar Basin, NW China. J. Asian Earth Sci. 194, 104222.

Gong, Z., Li, M., 2020. Astrochronology of the Ediacaran Shuram carbon isotope excursion, Oman. Earth Planet. Sci. Lett. 547, 116462.

Guo, P., Wen, H., Li, C., Jin, J., Lei, H., 2021. Origin and enrichment of borates in a Late Paleozoic alkaline lake-playa deposit, Junggar Basin, NW China. Ore Geol. Rev. 138, 104389.

Haq, B.U., Schutter, S.R., 2008. A Chronology of Paleozoic Sea-Level Changes. Science 322, 64–68.

Hayes, J.M., Strauss, H., Kaufman, A.J., 1999. The abundance of ^{13}C in marine organic matter and isotopic fractionation in the global biogeochemical cycle of carbon during the past 800 Ma. Chem. Geol. 161, 103–125.

He, D., Zhang, L., Wu, S., Li, D., Zhen, Y., 2018. Structural evolution stages and characteristics of Junggar Basin. Oil Gas Geol. 39, 845–861.

Hinnov, L.A., Diecchio, R.J., 2020. Upper Ordovician Juniata Formation, Central Appalachian Basin, USA: A record of Milankovitch-forced eustatic oscillations originating from glaciations in polar Gondwana. The Appalachian Geology of John M. Dennison: Rocks, People, and a Few Good Restaurants along the Way.

Hinnov, L.A., 2012. Cyclostratigraphy And Its Revolutionizing Applications in The Geosciences.

Huang, H., Gao, Y., Ma, C., Niu, L., Dong, T., Tian, X., Cheng, H., Hei, C., Tao, H., Wang, C., 2021. Astronomical constraints on the development of alkaline lake during the Carboniferous-Permian Period in North Pangea. Global Planet Change 207, 103681.

Isbell, J.L., Miller, M.F., Wolfe, K.L., Lenaker, P.A., Chan, M.A., Archer, A.W., 2003. Timing of late Paleozoic glaciation in Gondwana; was glaciation responsible for the development of Northern Hemisphere cyclothems? Special papers (Geol. Soc. Am. Bull.) 370, 5–24.

Jiang, F., Huang, R., Hu, T., Lv, J., Huang, L., Jiang, Z., et al., 2022. Geological characteristics and classification evolution of shale oil in Fengcheng Formation in Mahu Sag, Junggar Basin. Acta Petrolei Sinica 43 (7), 899–911.

Jin, S., Cao, H., Wang, H., Wagreich, M., Richoz, S., 2019. Orbital cyclicity in sedimentary sequence and climatic indications of C-O isotopes from Lower Cretaceous in Qingxi Sag, Jiuquan Basin, NW China. Geosci. Front. 10, 467–479.

Kodama, K., Hinnov, L., 2015. Rock Magnetic Cyclostratigraphy.

Kuang, L., Dong, D., He, W., Wen, S., Sun, S., Shuxin, L., Qiu, Z., Liao, X., Li, Y., Wu, J., Zhang, L., Shi, Z., Guo, W., Zhang, S., 2020. Geological characteristics and development potential of transitional shale gas in the east margin of the Ordos Basin, NW China. Petrol. Explor. Dev+ 47, 471–482.

Kump, L. R., Arthur M. A., 1999. Interpreting carbon-isotope excursions: carbonates and organic matter. 161, 198.

Laskar, J., Robutel, P., Joutel, F., Gastineau, M., Correia, A.C.M., Levrard, B., 2004. A long-term numerical solution for the insolation quantities of the Earth. Astron. Astrophys. 428, 261–285.

Laskar, J., Fienga, A., Gastineau, M., Manche, H., 2011. La2010: a new orbital solution for the long-term motion of the Earth. Astron. Astrophys. 532, A89.

Li, M., Hinnov, L. A., Huang, C., Ogg, J. G., 2018b. Sedimentary noise and sea levels linked to land–ocean water exchange and obliquity forcing. Nat. Commu. 9.

Li, M., Kump, L.R., Hinnov, L.A., Mann, M.E., 2018a. Tracking variable sedimentation rates and astronomical forcing in Phanerozoic paleoclimate proxy series with evolutionary correlation coefficients and hypothesis testing. Earth Planet. Sci. Lett. 501, 165–179.

Li, M., Huang, C., Ogg, J., Zhang, Y., Hinnov, L., Wu, H., Chen, Z., Zou, Z., 2019a. Paleoclimate proxies for cyclostratigraphy; comparative analysis using a Lower Triassic marine section in south China. Earth Sci. Rev. 189, 125–146.

Li, M., Hinnov, L., Kump, L., 2019b. Acycle: Time-series analysis software for paleoclimate research and education. Computat. Geosci. 127, 12–22.

Lisiecki, L.E., Raymo, M.E., 2005. A Pliocene-Pleistocene stack of 57 globally distributed benthic $\delta^{18}O$ records. Paleoceanography 20.

Liu, Y., Lo, L., Shi, Z., Wei, K., Chou, C., Chen, Y., Chuang, C., Wu, C., Mii, H., Peng, Z., Amakawa, H., Burr, G.S., Lee, S., DeLong, K.L., Elderfield, H., Shen, C., 2015. Obliquity pacing of the western Pacific Intertropical Convergence Zone over the past 282,000 years. Nat. Commu. 6.

Liu, B., Han, B., Chen, J., Ren, R., Zheng, B., Wang, Z., Feng, L., 2017. Closure time of the Junggar-Balkhash Ocean: Constraints from Late Paleozoic volcano-sedimentary sequences in the Barleik Mountains, West Junggar, NW China. Tectonics 36, 2823–2845.

Liu, Y., Wang, X., Wu, K., Chen, S., Shi, Z., Yao, W., 2019. Late Carboniferous seismic and volcanic record in the northwestern margin of the Junggar Basin: Implication for the tectonic setting of the West Junggar. Gondwana Res. 71, 49–75.

Lu, J., Wang, Y., Yang, M., Shao, L., Hilton, J., 2021. Records of volcanism and organic carbon isotopic composition ($\delta^{13}Corg$) linked to changes in atmospheric pCO_2

and climate during the Pennsylvanian icehouse interval. Chem. Geol. 570, 120168.
Ma, C., Li, M., 2020. Astronomical time scale of the Turonian constrained by multiple paleoclimate proxies. Geosci. Front. 11, 1345–1352.
Ma, C., Meyers, S.R., Sageman, B.B., 2019. Testing Late Cretaceous astronomical solutions in a 15 million year astrochronologic record from North America. Earth Planet. Sci. Let. 513, 1–11.
Mann, M.E., Lees, J.M., 1996. Robust estimation of background noise and signal detection in climatic time series. Clim. Change 33, 409–445.
Marwick, T.R., Borges, A.V., Van Acker, K., Darchambeau, F., Bouillon, S., 2014. Disproportionate Contribution of Riparian Inputs to Organic Carbon Pools in Freshwater Systems. Ecosystems 17, 974–989.
Meyers, S.R., 2015. The evaluation of eccentricity-related amplitude modulation and bundling in paleoclimate data: An inverse approach for astrochronologic testing and time scale optimization. Paleoceanography 30, 1625–1640.
Michel, L.A., Tabor, N.J., Montañez, I.P., Schmitz, M.D., Davydov, V.I., 2015. Chronostratigraphy and Paleoclimatology of the Lodève Basin, France: Evidence for a pan-tropical aridification event across the Carboniferous-Permian boundary. Palaeogeogr. Palaeoclimatol. Palaeoecol. 430, 118–131.
Montañez, I.P., Poulsen, C.J., 2013. The late Paleozoic ice age; an evolving paradigm. Annu. Rev. Earth. Pl. Sc. 41, 629–656.
Nordt, L., Tubbs, J., Dworkin, S., 2016. Stable carbon isotope record of terrestrial organic materials for the last 450 Ma yr. Earth Sci. Rev. 159, 103–117.
Paillard, D., Labeyrie, L., Yiou, P., 1996. Macintosh Program performs time-series analysis. EOS Trans. 77, 379.
Peters-Kottig, W., Strauss, H., Kerp, H., 2006. The land plant $\delta^{13}C$ record and plant evolution in the Late Palaeozoic. Palaeogeogr. Palaeoclimatol. Palaeoecol. 240, 237–252.
Phillips, T.L., Peppers, R.A., 1984. Changing patterns of Pennsylvanian coal-swamp vegetation and implications of climatic control on coal occurrence. Int. J. Coal Geol. 3, 205–255.
Ponton, C., West, A.J., Feakins, S.J., Galy, V., 2014. Leaf wax biomarkers in transit record river catchment composition. Geophy. Res. Lett. 41, 6420–6427.
Ramezani, J., Schmitz, M., Davydov, V., Bowring, S., Snyder, W., Northrup, C., 2007. High-precision U-Pb zircon age constraints on the Carboniferous-Permian boundary in the southern Urals stratotype. Earth Planet. Sci. Lett. 256, 244–257.
Sengor, A.M.C., Natalin, B., Burtman, V., 1993. Evolution of the Altaid Tectonic collage and Palaeozoic Crustal Growth in Eurasia. Nature 364.
Shi, J., Jin, Z., Liu, Q., Zhang, R., Huang, Z., 2019. Cyclostratigraphy and astronomical tuning of the middle eocene terrestrial successions in the Bohai Bay Basin, Eastern China. Global Planet Change 174, 115–126.
Shi, J., Jin, Z., Liu, Q., Fan, T., Gao, Z., 2021. Sunspot cycles recorded in Eocene lacustrine fine-grained sedimentary rocks in the Bohai Bay Basin, eastern China. Global Planet Change 205, 103614.
Strasser, A., Hilgen, F.J., Heckel, P.H., 2006. Cyclostratigraphy - concepts, definitions, and applications. Newsl. Stratigr. 42, 75–114.
Tang, Y., Cao, J., He, W., Guo, X., Zhao, K., Li, W., 2021b. Discovery of shale oil in alkaline lacustrine basins: The Late Paleozoic Fengcheng Formation, Mahu Sag, Junggar Basin, China. Petrol. Sci. 18, 1281–1293.
Tang, W., Zhang, Y., Pe-Piper, G., Piper, D.J.W., Guo, Z., Li, W., 2021a. Permian rifting processes in the NW Junggar Basin, China: Implications for the post-accretionary successor basins. Gondwana Res. 98, 107–124.
Thomson, D. J., 1982. Spectrum estimation and harmonic analysis. Proc. IEEE.
Torrence, C., Compo, G.P., 1998. A Practical Guide to Wavelet Analysis. B. Am. Meteorol. Soc. 79, 61–78.
Waltham, D., 2015. Milankovitch Period Uncertainties and Their Impact on Cyclostratigraphy. J. Sediment. Res. 85, 990–998.
Wan, Y., Feng, Q., Liu, Y., Tabor, N., Dan, M., Crowley, J.L., Lin, J., Thomas, S., 2010. Depositional environments and cyclo- and chronostratigraphy of uppermost Carboniferous-Lower Triassic fluvial–lacustrine deposits, southern Bogda Mountains, NW China - A terrestrial paleoclimatic record of mid-latitude NE Pangea. Global Planet Change 73, 15–113.
Wang, X., Auler, A.S., Edwards, R.L., Cheng, H., Cristalli, P.S., Smart, P.L., Richards, D. A., Shen, C., 2004. Wet periods in northeastern Brazil over the past 210 kyr linked to distant climate anomalies. Nature 432, 740–743.
Wang, T., Cao, J., Xia, L., Zhi, D., Tang, Y., He, W., 2022. Revised age of the Fengcheng Formation, Junggar Basin, China: Global implications for the late Paleozoic ice age. Global Planet Change 208, 103725.
Wang, M., Chen, H., Huang, C., Kemp, D.B., Xu, T., Zhang, H., Li, M., 2020a. Astronomical forcing and sedimentary noise modeling of lake-level changes in the Paleogene Dongpu Depression of North China. Earth Planet. Sci. Lett. 535, 116116.
Wang, T., Cao, J., Carroll, A., Zhi, D., Tang, Y., Wang, X., Li, Y., 2020b. Oldest Preserved Sodium Carbonate Evaporite: Late Paleozoic Fengcheng Formation, Junggar Basin, NW China. GSA Bulletin 133.
Wang, X., Hu, K., Shi, Y., Chen, J., Yang, S., Ye, X., Li, X., Song, Y., Chen, B., Chang, X., Yao, L., Zhang, Y., Fan, J., Shen, S., 2021. The missing upper Carboniferous in the Cimmerian continent: A critical review. Earth Sci. Rev. 217, 103627.
Wu, H., Fang, Q., Wang, X., Hinnov, L.A., Qi, Y., Shen, S.Z., Yang, T., Li, H., Chen, J., Zhang, S., 2018. An ~34 m.y. astronomical time scale for the uppermost Mississippian through Pennsylvanian of the Carboniferous System of the Paleo-Tethyan realm. Geology.
Yu, K., Cao, Y., Qiu, L., Sun, P., Jia, X., Wan, M., 2018. Geochemical characteristics and origin of sodium carbonates in a closed alkaline basin: The Lower Permian Fengcheng Formation in the Mahu Sag, northwestern Junggar Basin, China. Palaeogeogr. Palaeoclimatol. Palaeoecol. 511, 506–531.
Zachos, J., Shackleton, N., Revenaugh, J., Pälike, H., Flower, B., 2001. Climate Response to Orbital Forcing Across the Oligocene-Miocene Boundary. Science 292, 274–278.
Zhi, D., Song, Y., He, W., Jia, X., Zou, Y., Huang, L., 2019. Geological characteristics, resource potential and exploration direction of shale oil in Middle-Lower Permian, Junggar Basin. Xinjiang Petrol. Geol. 40, 389–401.